The Biosynthesis of Flavin Cofactors in *Listeria monocytogenes*

Maria Sebastián [1], Sonia Arilla-Luna [1], Jacques Bellalou [2], Inmaculada Yruela [3,4] and Milagros Medina [1,4]

1 - Departamento de Bioquímica y Biología Molecular y Celular, *Facultad de Ciencias and Instituto de Biocomputación y Física de Sistemas Complejos, Universidad de Zaragoza, 50009 Zaragoza, Spain*
2 - Plateforme de Protéines Recombinantes, *Institut Pasteur, CNRS-UMR 3528, Paris, France*
3 - Estación Experimental de Aula Dei, *National Spanish Research Council (CSIC), Zaragoza, Spain*
4 - Group of Biochemistry, *Biophysics and Computational Biology (BIFI-Unizar) Joint Unit to CSIC Spain*

Correspondence to Milagros Medina: *Departamento de Bioquímica y Biología Molecular y Celular, Facultad de Ciencias, Universidad de Zaragoza, Pedro Cerbuna, 12, 50009 Zaragoza, Spain. mmedina@unizar.es*
https://doi.org/10.1016/j.jmb.2019.05.029
Edited by Anthony Maxwell

Abstract

Listeria monocytogenes is riboflavin auxotrophic, but it has two genes envisaged to transform riboflavin into FMN and FAD after its uptaked by specialized transporters. One encodes a bifunctional type I FAD synthase (FADS, herein *Lm*FADS-1), while the other produces a protein similar to type I at the FMN:ATP adenylyltransferase (FMNAT) site but with a shorter C-terminal that lacks any riboflavin kinase (RFK) motif. This second protein is rare among bacteria and has been named FADS type II (*Lm*FADS-2). Here we present a biochemical and biophysical study of *Lm*FADS-1 and *Lm*FADS-2 by integrating kinetic and thermodynamic data together with sequence and structural prediction methods to evaluate their occurrence in *Listeria*, as well as their function and molecular properties. Despite *Lm*FADS-1 similarities to other type I FADSs, (i) its RFK activity has not riboflavin substrate inhibition and occurs under reducing and oxidizing conditions, (ii) its FMNAT activity requires strong reducing environment, and (iii) binding of reaction products, but not substrates, favors binding of the second ligand. *Lm*FADS-2 produces FAD under oxidizing and reducing environments, but its C-terminus module function remains unknown. *Listeria* species conserve both FADSs, being sequence identity high within *L. monocytogenes* strains. Our data exemplify alternative strategies for FMN and FAD biosynthesis and homeostasis, envisaging that in *Listeria* two FADSs might be required to fulfill the supply of flavin cofactors under niches that can go from saprophytism to virulence. As FADSs are attractive antimicrobial targets, understanding of FADSs traits in different species is essential to help in the discovery of specific antimicrobials.

Introduction

Listeria monocytogenes is a gram-positive facultative intracellular human pathogen that causes listeriosis, a severe human infection with a high mortality rate and involved in numerous outbreaks due to contaminated food [1,2]. It is responsible for 20%–30% of all food related deaths involving known foodborne pathogens [1,3]. Infection with *L. monocytogenes* is often associated with severe disease in pregnant women, neonates, the elderly, and immunosuppressed patients [4–6]. *L. monocytogenes* inhabits numerous ecological niches, being able to multiply at broad ranges of pH (4.5–9) and temperature (0–45 °C), as well as at high salt concentrations (10% NaCl). It also has the ability to invade and replicate within a variety of human and animal host cells, what makes listeriosis treatment problematic [2,7,8]. In addition, identification of food products contaminated with this bacteria (usually dairy products, fish, poultry, meat, …) remains challenging [9].

The *L. monocytogenes* genome contains two genes that codify for enzymes involved in the biosynthesis of flavin cofactors [10,11]. Both of them are involved in

the transformation of the riboflavin precursor (vitamin B_2, RF) into the FMN and FAD cofactors used by flavoproteins and flavoenzymes [11]. Therefore *L. monocytogenes* strains are auxotrophic for RF [12], relying on the presence of RF transporters to provide this nutrient [13,14]. In a previous phylogenetic study, we showed that one of these genes codifies for a canonical type I prokaryotic bifunctional FAD synthase (FADS) (herein *Lm*FADS-1 for *L. monocytogenes*) [15]. Type I FADSs fold in two modules. The N-terminal module holds an FMN:ATP adenylyltransferase activity (FMNAT, EC 2.7.7.2) that transforms FMN into FAD, being this reaction reversible in some species [FAD pyrophosphorylase activity (FADpp)] [16–18]. On its side, the C-terminal module has riboflavin kinase (RFK, EC 2.7.1.26) activity and is responsible for the transformation of RF into FMN. The second *L. monocytogenes* gene related to the biosynthesis of flavins codifies for a protein with significant similarity to type I FADSs in the N-terminal module, but with a shorter C-terminal module that lacks the RFK consensus PTAN motif. This form was labeled as type II FADS (herein *Lm*FADS-2 for *L. monocytogenes*) and was expected to hold FMNAT activity but not RFK activity [15]. A recent study using type I and type II proteins of the *L. monocytogenes* EGD-e strain showed that, whereas the type I enzyme produces FMN and FAD, the type II only produces FAD [11]. Detailed biochemical, structural, and biophysical characterization of prokaryotic FADSs is, however, reduced to the type I enzymes from *Corynebacterium ammoniagenes* (*Ca*FADS) and *Streptococcus pneumoniae* (*Spn*FADS) [16,17,19–27], while the rest of the family members have been either not studied at all or hardly characterized [11,28,29]. Furthermore, prokaryotic FADSs are attractive exploitable targets for the treatment of infections due to differences in chemistry and structure for the transformation of FMN into FAD when compared to the eukarya, particularly mammalian enzymes catalyzing this transformation [19,22,30,31]. Therefore, we consider worthwhile the characterization of the two *L. monocytogenes* enzymes.

We present here the biochemical and biophysical characterization of *Lm*FADS-1 and *Lm*FADS-2 from *L. monocytogenes* HCC23. Our data confirm that *Lm*FADS-1 catalyzes the RFK, FMNAT, and FADpp activities, while *Lm*FADS-2 only has FMNAT and FADpp activities. Despite the overall functional and predicted structural similarities among *Lm*FADS-1 and other members of the FADS family, this protein presents two catalytic particularities: (i) its RFK activity does not exhibit inhibition by the RF substrate and it takes place both under reducing and oxidizing conditions—although the catalytic efficiency is different—and (ii) *Lm*FADS-1 requires strong reducing conditions for its FMNAT activity, as previously shown for *Spn*FADS [16], but not for *Ca*FADS. On its part, *Lm*FADS-2 is able to transform FMN into FAD both under oxidizing and reducing conditions. While sequence and structural analysis allow us to envisage key structural aspects for FMNAT and/or RFK catalysis in *Lm*FADS-1 and *Lm*FADS-2, they hardly shed light on the potential function of the *Lm*FADS-2 C-terminus module. Nonetheless, occurrence of *Lm*FADS-2 is also analyzed in the context of some particular *Listeria* traits. Finally, the results here presented, when evaluated in the context of the knowledge of other FADS family members, further contribute to exemplify the alternative strategies adopted by different organisms to carry out the same reactions, supporting *Lm*FADSs as potential drug targets, due to their differences regarding other prokaryotic FADSs as well as the human proteins that synthesize FMN and FAD.

Results

The monomer is the most populated state for *Lm*FADS-1 and *Lm*FADS-2, but both stabilize some homo-oligomers

The heterologous overexpression of *Lm*FADS-1 and *Lm*FADS-2 in *Escherichia coli* cells using conventional orbital incubators produced proteins that mostly accumulate into inclusion bodies, while the use of a Bioflo3000 fermenter with a strict control of main parameters of culivation increased the proportion of soluble proteins (Fig. SP1). This highlighted the relevance of oxygenation to reach high cell density and of the use of low tempertaures during the induction phase, in the expression and folding of these two proteins. SDS-PAGE confirmed purification to homogeneity and allowed to predict apparent molecular weights (MW) of 37 and 35 kDa for *Lm*FADS-1 and *Lm*FADS-2, respectively (corresponding theoretical values 35.6 and 27.7 kDa). Typically, the yield after purification was ~3.5 mg of *Lm*FADS-1 and ~2.5 mg of *Lm*FADS-2 per g of *E. coli* cells. Both purified proteins were relatively unstable, tending to aggregate and to precipitate after 3–4 weeks of their purification. Therefore, only freshly purified samples (less than 2 weeks) were used to carry out the experiments herein reported. To guaranty reproducibility and stability, changes in the medium were minimized, while protein solubility and catalytic efficiency were tested before and after each analysis. We used gel filtration chromatography to further characterize their apparent MWs, as well as their ability to stabilize quaternary organizations. *Lm*FADS-1 eluted as a main peak with an apparent MW of 52 kDa (Fig. SP2A). The discrepancy between this value and the theoretical one could be explained because *Lm*FADS-1 is predicted to be an elongated shaped protein, and

therefore, its hydrodynamic volume is higher than expected, as reported for other type I FADSs [32]. Apart from the monomer peak, three minority species were detected with apparent MW around twice, three, and six times the weight of the monomeric species. For its part, *Lm*FADS-2 eluted as a main peak of MW ~25.7 kDa (Fig. SP2B), which agrees with the monomer theoretical MW, indicating that *Lm*FADS-2 is more compact and globular than *Lm*FADS-1. We also detected two considerably less relevant populations twice and four times heavier than the *Lm*FADS-2 monomer. Consequently, the monomer is the most populated state for both proteins under the evaluated conditions, but they might also stabilize homo-oligomers that contain different number of protomers.

*Lm*FADS-1 and *Lm*FADS-2 can be purified as folded proteins able to internalize flavins in the absence of adenine nucleotides

The UV–visible spectra of *Lm*FADS-1 and *Lm*FADS-2 presented a single absorption maximum at 279 nm, indicating that the purified protein lacks of any bound flavin or adenine nucleotide. The $\varepsilon_{279\ nm}$ determined under the assayed conditions were 27.9 and 28.5 mM^{-1} cm^{-1}, respectively. Deviations from the theoretical values—34.8 and 26.9 mM^{-1} cm^{-1}, respectively—suggest changes in the environment of some aromatic residues upon folding.

Far-UV circular dichroism (CD) spectra showed a broad negative band with minima at 209 and 216 nm for both proteins (Fig. 1a), revealing β-sheets and α-helices as secondary structure elements. Near-UV CD spectra displayed a wide negative 265–300 nm band, with signal magnitude and hyperfine structure differing between both proteins (Fig. 1b). This agress with different content of aromatic residues (*Lm*FADS-1, 16 Tyr, 16 Phe and 2 Trp; *Lm*FADS-2, 7 Tyr, 8 Phe and 3 Trp) and indicates their dissimilar internalization in tertiary structures.

*Lm*FADS-1 and *Lm*FADS-2 yielded visible difference spectra when titrated with oxidized RF, FMN, and FAD, which indicate that both proteins are able to directly interact with these flavins in their oxidized states. Nevertheless, differences between both proteins are observed in the magnitude and position of the peaks. Spectral changes when titrating *Lm*FADS-1 with RF and FMN are similar; maxima at 388 and 495 nm, the later with a shoulder at 466 nm, and minima at 357 and 435–438 nm (Fig. 2a). Titration with FAD produced a slightly different spectrum (Fig. 2a); a minimum at 434 nm and maxima at 498 and 466 nm, pointing to a distinct environment of the FAD isoalloxazine ring. When titrating with RF and, particularly, with FMN the *Lm*FADS-1:ADP complex (Fig. 2b)—protein saturated with ADP—we observed an noticeable magnitude increase of the difference spectra peaks, while the titration with FAD did not present this effect. This fact indicates that the adenine nucleotide favors the RF and FMN binding but not FAD binding, suggesting that, as in other type I FADSs, the adenine nucleotide favors flavin binding at the RFK site [20]. In the case of *Lm*FADS-2, titrations with RF, FMN, or FAD yielded weaker difference spectra (Fig. 2c). However, all spectra showed two maxima—409, 407, or 413 nm and 488, 487, or 489 nm, respectively—and two minima—366, 355, or 382 nm and 440, 443, or 446 nm, respectively. In addition, titrations with RF and FAD yielded a broad maximum at 335 and 342 nm, respectively. Noticeably, no difference spectra were detected when titrating a mixture containing *Lm*FADS-2 and excess of ADP with RF (Fig. 2d). Despite ADP is neither a substrate nor a product for the FMANT reaction, we used it to mimic the binding of the ATP substrate. Since ADP

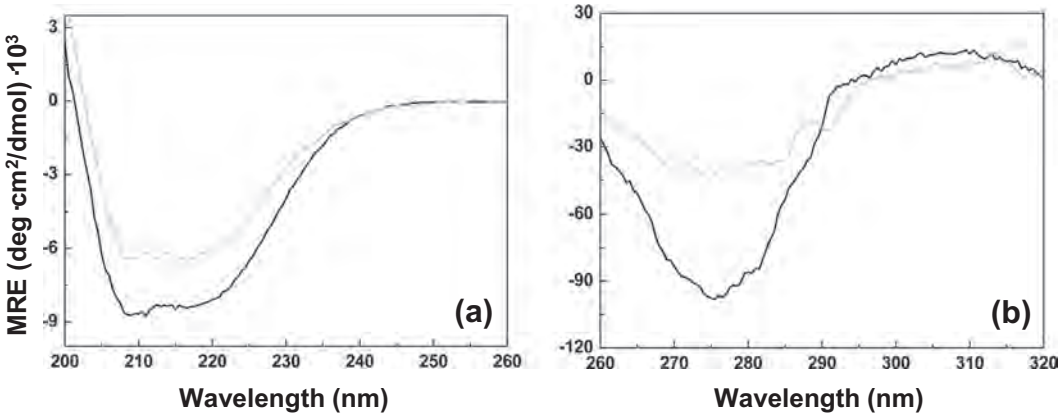

Fig. 1. Circular dichroism spectra for *Lm*FADS-1 and *Lm*FADS-2. Molar ellipticity *per* residue (a) in the far-UV region and (b) in the near-UV region. *Lm*FADS-1 and *Lm*FADS-2 are shown in black and gray lines, respectively. Spectra registered in 20 mM Pipes (pH 7.0) at 15 °C.

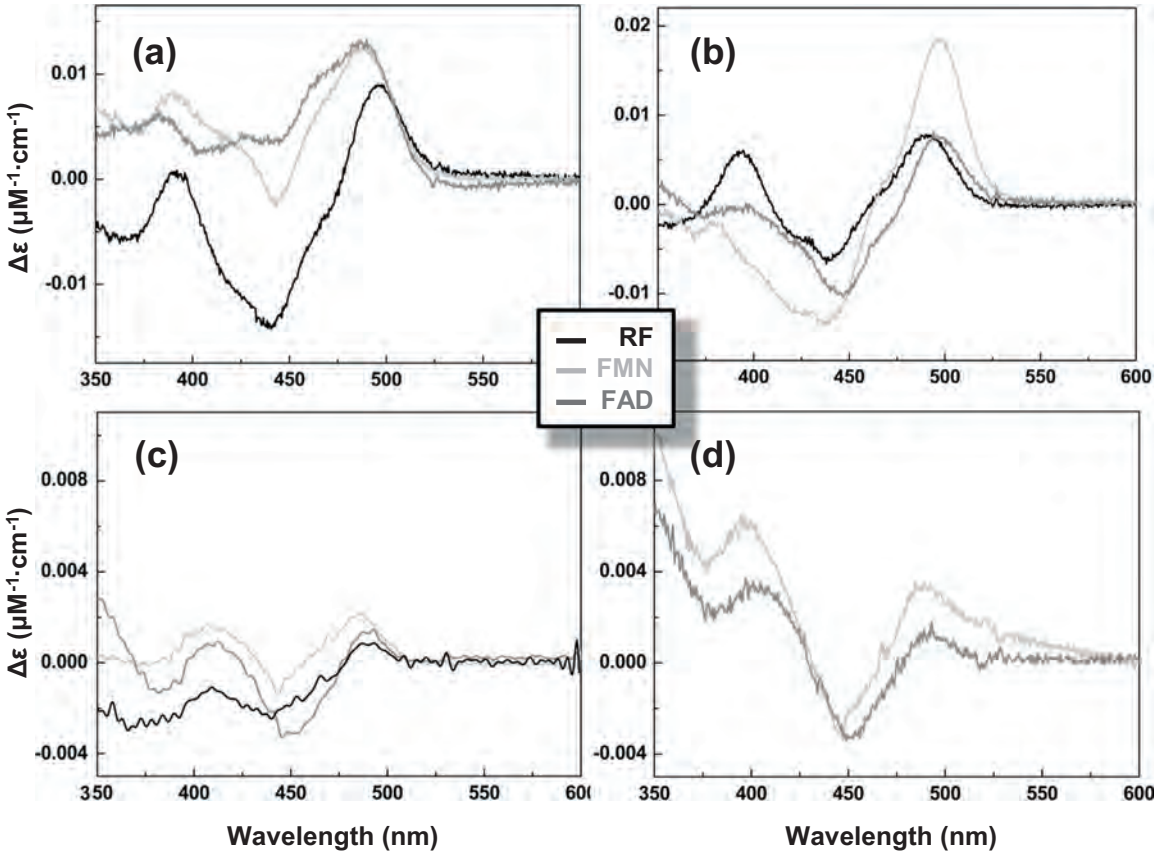

Fig. 2. Visible difference spectra obtained upon titration of *Lm*FADS-1 and *Lm*FADS-2 with flavin cofactors. Titration of samples containing (a) *Lm*FADS-1, (b) a mixture of *Lm*FADS-1 with excess of ADP, (c) *Lm*FADS-2, and (d) a mixture of *Lm*FADS-2 with excess of ADP with saturating concentrations of RF (black line), FMN (light gray line), and FAD (dark gray line). Initial protein concentration was 5 μM and when present ADP was at 200 μM. Spectra registered at 15 °C in 20 mM Pipes, 10 mM $MgCl_2$, and 7 mM imidazole (pH 7.0). No difference spectrum was detected when titrating the *Lm*FADS-2:ADP complex with RF. Shown spectra are the saturation ones.

binding to the FMANT module in type I FADSs has been proven [20], we expected it to bind to *Lm*FADS-2, although we have not been able to proof it yet. Nonetheless, if ADP binding happens, our results would agree with previous studies indicating that ADP favors flavin binding at the RFK site of type I FADS, while its binding to the FMNAT site hardly has effect on flavin binding [20].

The redox status of the media modulates catalytic activities of *Lm*FADS enzymes

The ability of *Lm*FADS-1 and *Lm*FADS-2 to transform RF, FMN, and FAD under different conditions was qualitatively evaluated using thin layer chromatography (TLC) (Fig. SP3). *Lm*FADS-1 showed RFK, FMNAT, and FADpp activities, confirming that it is a bifunctional FADS, although it requires strong reducing conditions to catalyze the FMNAT and FADpp reactions. *Lm*FADS-2 did not show RFK activity but catalyzes the FMNAT and FADpp activities—both located at the FMNAT module—under both oxidizing and reducing conditions.

Kinetic parameters for the RFK activity of *Lm*FADS-1 (Fig. 3) yielded k_{cat} and K_m^{RF} values 3-fold and 20-fold larger, respectively, when determined under reducing conditions, while K_m^{ATP} decreased by 3-fold (Table 1). Therefore, the media redox status modulates the RFK catalytic efficiency by particularly acting on the K_m. Under oxidizing conditions, the lower K_m^{RF} when compared with K_m^{ATP} makes the transformation of this flavin by *Lm*FADS-1 highly efficient. Under reducing conditions, K_m values for both substrates are similar. The consequence is a negative impact in the catalytic efficiency regarding RF, making similar the efficiency for the transformation of both substrates.

*Lm*FADS-1 only exhibited FMNAT activity under strong reducing conditions (Fig. 4a and b), while *Lm*FADS-2 transformed FMN into FAD both under oxidizing and reducing environments (Fig. 4c and d).

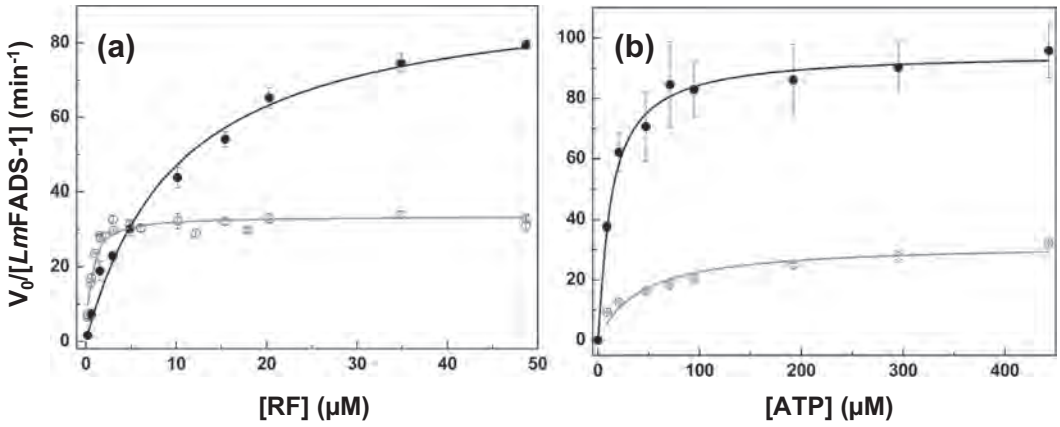

Fig. 3. Michaelis–Menten plots for the *Lm*FADS-1 RFK activity. (a) ATP and (b) RF saturating concentrations when, respectively, varying RF and ATP concentrations. Profiles were obtained under reducing conditions (24 mM dithionite, dots and lines in black) and under oxygen atmosphere (dots and lines in gray). Reactions carried out in 20 mM Pipes and 0.8 mM $MgCl_2$ (pH 7.0).

*Lm*FADS-1 has a high k_{cat} value but mild efficiency as a consequence of relatively high K_m values (Table 2). *Lm*FADS-2 showed similar kinetic parameters regardless the redox environment (Table 2), being only K_m^{ATP} smaller in oxidizing environment. This makes *Lm*FADS-2 more efficient under oxidizing conditions.

Thermodynamics explain regulation of the *Lm*FADS-1 catalytic activities by the reaction products

We then moved to determine the thermodynamic parameters for the interaction of *Lm*FADS-1 and *Lm*FADS-2 with all their ligands by using isothermal titration calorimetry (ITC). We performed two types of experiments, first we titrated the free protein with a single ligand, and then we titrated pre-formed mixtures, with either flavin or adenine nucleotides, with a nucleotide of different nature. Furthermore, we carried out all titrations under aerobic conditions and both in presence and absence of Mg^{2+} to evaluate the effect of this cation.

*Lm*FADS-1 is able to produce binary complexes with all of its ligands and Mg^{2+}. In general, Mg^{2+} only slightly modifies their affinity, as the K_d and ΔG values with and without Mg^{2+} indicate (Fig. 5 and Table SP1). Noticeably, when titrating with a single substrate, the cation presence considerably enhanced the enthalpic contribution to the binding. Mg^{2+} also favored the formation of ternary complexes, *Lm*FADS-1:ANP:FLV (where ANP refers to ATP or ADP, and FLV to RF or FMN), over the binary ones, as their lower positions in the free energy diagram show (Fig. 5). When analyzing the enthalpic and entropic fingerprints to the binding—with and without Mg^{2+}—(Table SP1), it is stated that the increase in complex stability is due to the more favorable enthalpic contribution to the binding in presence of this cation. Altogether these facts reveal that the cation has an active role in the establishment of specific interactions of substrates with *Lm*FADS-1.

Although we could not titrate *Lm*FADS-1 with the substrates of the RFK activity in presence of Mg^{2+}—the reaction would mask the interaction heat—we were able to evaluate ternary complexes with RF and ATP in its absence (Fig. 5A), leading to the formation of pseudo-catalytic *Lm*FADS-1:RF:ATP complexes. As the position of the catalytic complex in the free energy diagram shows, other ternary complexes are more favored from the thermodynamic point of view, deserving special attention those with FMN. As demonstrated for other FADS family members, this fact suggests the inhibitory regulation of the *Lm*FADS-1 catalytic activities by the products of the RFK reaction. Such an hypothesis is

Table 1. Kinetic parameters for the RFK activity of *Lm*FADS-1

	k_{cat} (min^{-1})	K_m^{RF} (μM)	K_m^{ATP} (μM)	k_{cat}/K_m^{RF} (min^{-1} μM^{-1})	k_{cat}/K_m^{ATP} (min^{-1} μM^{-1})
*Lm*FADS-1 (–)	33 ± 2	0.5 ± 0.1	41 ± 2	66 ± 4	0.8 ± 0.1
*Lm*FADS-1 (+)	95 ± 7	10 ± 1	12 ± 1	9.5 ± 0.8	7.9 ± 1

Experiments were performed in 20 mM Pipes and 0.8 mM $MgCl_2$ (pH 7.0) at 25 °C, both in the absence (–) and in the presence of 24 mM sodium dithionite (+) (n = 3; mean ± SD).

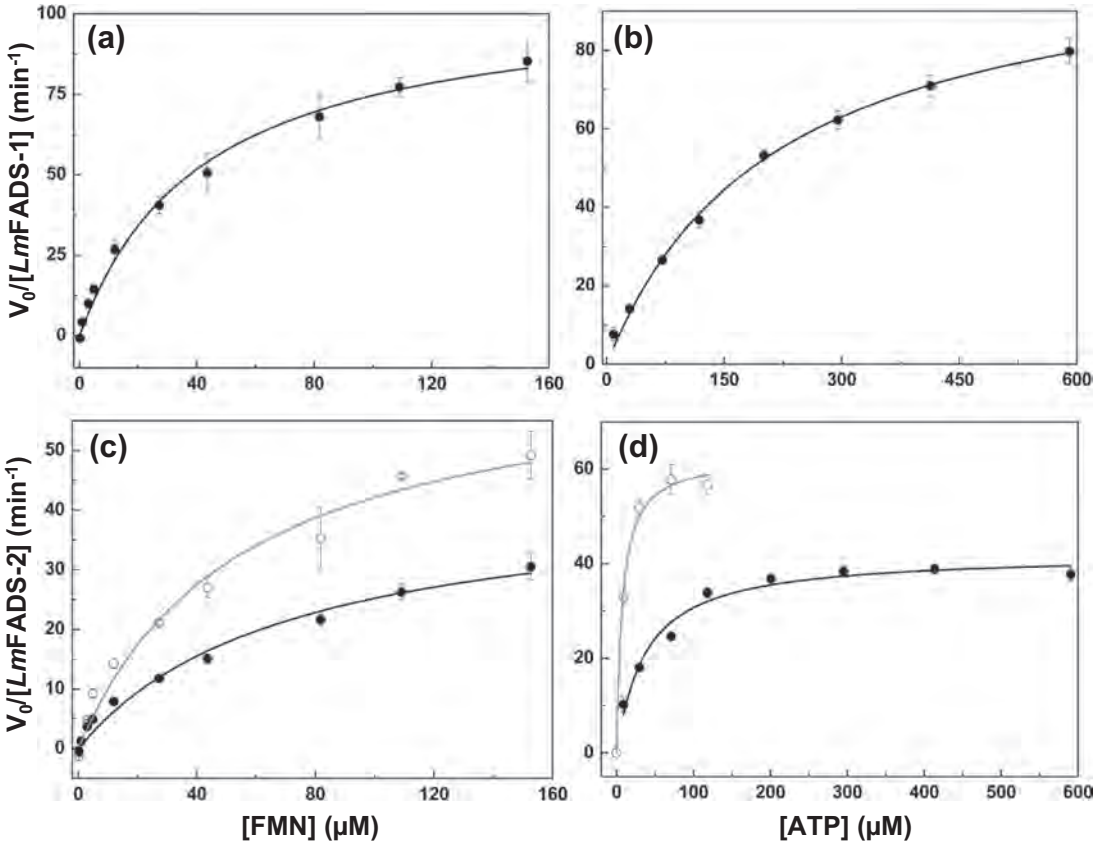

Fig. 4. Michaelis–Menten plots for the *Lm*FADS-1 and *Lm*FADS-2 FMNAT activities. Panels a and b show the *Lm*FADS-1 profiles at saturating concentrations of ATP and FMN, respectively, when varying the other substrate. Panels c and d show the *Lm*FADS-2 concentrations profiles at saturating ATP and FMN, respectively. Reactions were carried out under reducing conditions (24 mM sodium dithionite, dots and lines in black) and under oxygen atmosphere (dots and lines in gray).

also supported by the cooperation coefficients summrized in Table 3. Cooperation coefficients indicate how the fact that there is another substrate previously bound to the protein affects the binding of a ligand. The existence of a bound flavin or an adenine nucleotide strongly favored the binding of the second FLV/ANP ligand—both with and without Mg^{2+}—with the only exception of the RF/ATP combination (measured only in the absence of the cation), where the first ligand did not affect the binding of the second one.

Determination by ITC of the thermodynamic binding parameters for ligands binding to *Lm*FADS-2 was not possible, since the time required for these experiments was long and it was difficult to ensure protein preserving its full functionality under the assay conditions. This, together with the weak interaction of *Lm*FADS-2 with the flavin substrates envisaged by

Table 2. Kinetic parameters for the FMNAT activity of *Lm*FADS-1 and *Lm*FADS-2

	k_{cat} (min^{-1})	K_m^{FMN} (μM)	K_m^{ATP} (μM)	k_{cat}/K_m^{FMN} (min^{-1} μM^{-1})	k_{cat}/K_m^{ATP} (min^{-1} μM^{-1})
*Lm*FADS-1 (+)	108 ± 8	42 ± 3	215 ± 15	2.6 ± 0.2	0.5 ± 0.1
*Lm*FADS-2 (–)	65 ± 5	55 ± 5	7.4 ± 0.6	1.2 ± 0.2	8.8 ± 0.8
*Lm*FADS-2 (+)	43 ± 3	71 ± 6	37 ± 2	0.6 ± 0.1	2.0 ± 0.2

Experiments were performed in 20 mM Pipes and 0.8 mM $MgCl_2$ (pH 7.0) at 25 °C, both in the absence (–) and presence of 24 mM sodium dithionite (+) (n = 3; mean ± SD).

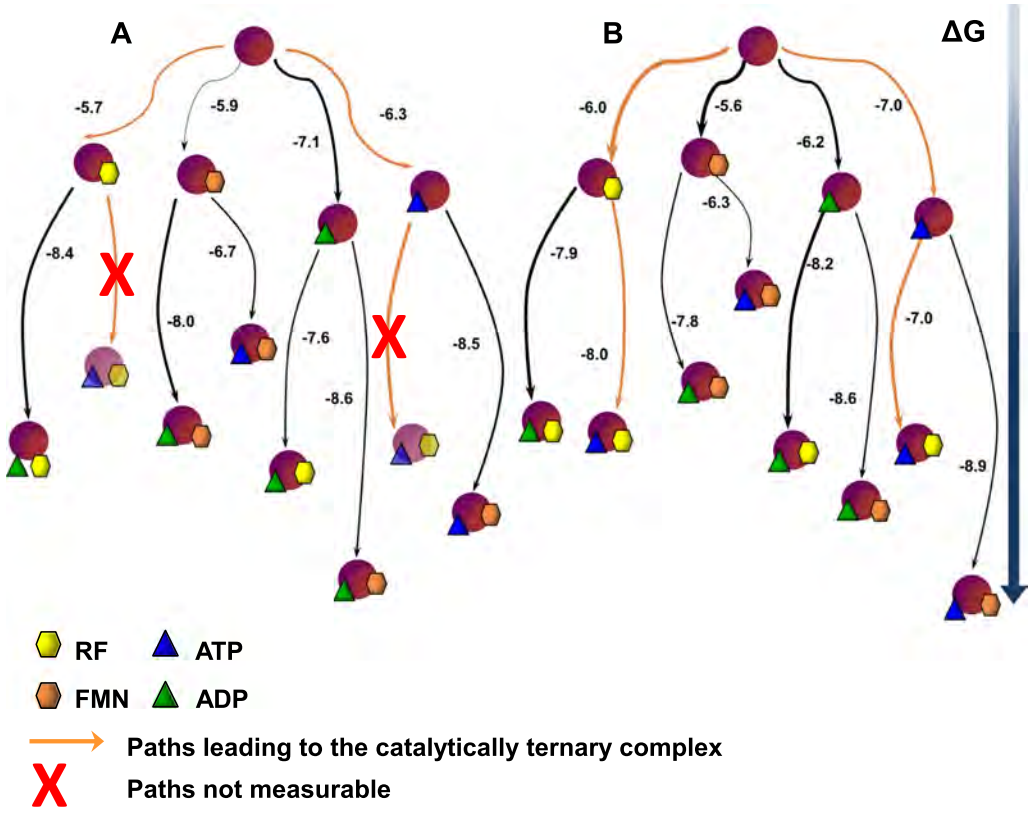

Fig. 5. Gibbs free energy flow for the interaction of *Lm*FADS-1 with ligands. Diagrams summarize the thermodynamic parameters obtained through ITC, for the interaction of *Lm*FADS-1 and different combinations of the substrates and products of its RFK activity. Data obtained at 15 °C in (A) 20 mM Pipes (pH 7.0) and 0.8 mM $MgCl_2$ and in (B) 20 mM Pipes (pH 7.0) and 0 mM $MgCl_2$. *Lm*FADS-1 is shown as maroon spheres, RF and FMN as yellow, and hexagons as orange, respectively, and ADP and ATP as green and blue triangles, respectively. Numbers display the free energy values obtained for each titration. The thickness of the arrows is proportional to the fraction of *Lm*FADS-1, which is binding the titrating ligand, while the length of the lines is directly proportional to the Δ*G* value for each process. The paths that lead to the ternary complex of the protein with the substrates of the RFK reaction, that is, RF and ATP, are shown in orange. Red crosses indicate processes that could not be measured in the presence of Mg^{2+} since the reaction heat would mask the interaction heat.

Table 3. Cooperation coefficients for the binding of different combinations of flavin and adenine nucleotides to *Lm*FADS-1, both in the absence (upper part of the table) and in the presence of 0.8 mM of Mg^{2+} (lower part of the table)

Ligands	*α*	*N*	Δ*h* (kcal mol^{-1})
0 mM Mg^{2+}			
FMN-ADP	65 ± 6	0.30 ± 0.01	6.1 ± 0.3
FMN-ATP	15 ± 2	0.30 ± 0.01	−7.5 ± 0.4
RF-ADP	6.8 ± 1.1	0.50 ± 0.01	3.7 ± 0.4
RF-ATP	1.0 ± 0.1	0.50 ± 0.02	−35 ± 3
0.8 mM Mg^{2+}			
FMN-ADP	15 ± 2	0.40 ± 0.01	8.8 ± 0.3
FMN-ATP	56 ± 7	0.40 ± 0.01	3.7 ± 0.3
RF-ADP	2.6 ± 0.5	0.30 ± 0.01	−2.4 ± 0.2
RF-ATP	[a]	[a]	[a]

α is the cooperation coefficient, *N* the fraction of total protein able to bind the titrating ligand, and Δ*h* the enthalpy change associated with each process. Experiments carried out in 20 mM Pipes (pH 7.0) at 15 °C (n = 3; mean ± SD).

[a] This combination of ligands in the presence of Mg^{2+} leads to the catalytic reaction, which prevents the determination of binding heats.

difference spectroscopy, highlights the soft nature of the interactions established by this protein.

The C-terminal module of *Lm*FADS-2 is rare among bacteria, predicted as unstructured and with not envisaged function

*Ca*FADS (pdb 2X0K) and *Spn*FADS (pdb 3OP1) x-ray structures are potential templates to model the proteins studied here. *Lm*FADS-1 shares up to 40% and 32% sequence identity with *Spn*FADS (*E*-value 4×10^{-66}) and *Ca*FADS (*E*-value 1×10^{-43}), respectively, with conserved residues covering all sequence (Fig. SP4). The N-terminal (residues 1–184) region of *Lm*FADS-2 also covers well the FMNAT module in *Spn*FADS (*E*-value 1.1×10^{-22}, 34% identity) and *Ca*FADS (*E*-value 5.7×10^{-25}, 30% identity). However, its C-terminal (residues 185–245) is more than 50 residues shorter than the RFK module of type I FADSs and lacks the consensus RFK catalytic PTAN

motif (Fig. SP4) [15]. The N-terminal regions of the *Lm*FADS-1 and *Lm*FADS-2 predicted secondary structures also show a high correspondence with the FMNAT module in type I FADSs (Fig. SP4). In addition, the predicted secondary structure for the *Lm*FADS-1 C-terminal module (residues 188–314) matches with the RFK module of type I FADSs, although, similarly to *Spn*FADS, lacks the ^{235}Glu-^{247}Ala extension present in *Ca*FADS. This potentially flexible extension is found only in sequences for *Corynebacterium* and *Mycobacterium* species [19,32] as part of loop L3c [21], which is predicted to be a determinant in the dimer-of-trimers assembly during RFK catalysis [32]. On the contrary, the *Lm*FADS-2 C-terminal region is envisaged to hold a poor content in secondary structure (Fig. SP4), lacking key structural elements for the RFK catalysis such as the PTAN motif, the β-barrel or the terminal α-helix. Our sequence analyses also identified potential recognitions sites (MoRFs regions) at the end of the C-terminal module, as well as variations in the predicted intrinsically disordered/ductile residues (IDRs) of the FADS sequences here evaluated (Fig. SP4). The proportion of IDRs apparently increases from *Ca*FADS (9.5%) to FADSs from pathogenic bacteria, *Spn*FADS (13.4%), *Lm*FADS-2 (14.7%), and *Lm*FADS-1 (16.9%). These percentages are similar to those found in *Mycobacterium tuberculosis* proteins (14%) [33].

Homology models for the FMNAT modules of *Lm*FADS-1 and *Lm*FADS-2, built using as templates the apoforms of *Ca*FADS and *Spn*FADS, result fairly similar (Fig. 6), with divergences reduced to loops conecting secondary structure elements. The most remarkable differences are located around the *Lm*FADS-1 C-terminal RFK active site, particularly in the conformation of the PTAN motif and the loops L1c and L5c that, according to other species, give the ATP substrate access to the active site (Figs. 6 and 7) [16,21]. Variance between our two models for the *Lm*FADS-1 RFK module relates to the different conformation of these elements in the templates [16,27]. In addition, in both *Lm*FADS-1 models, the L3c loop has a conformation similar to that of the *Spn*FADS template (Fig. 6). Finally, the lack of a sequence and secondary structure homology of the *Lm*FADS-2 C-terminal region to any known tertiary structure prevents us from producing a reliable model for this domain.

Discussion

Despite similarities among *Lm*FADSs and prokaryotic FADSs, *Lm*FADS-1, and, specifically, *Lm*FADS-2 show particularities that might lay bare the evolutionary divergences that force organisms to adopt different strategies to produce essential molecules. *Lm*FADS-1 is predicted to have all structural elements related to the RFK and FMNAT activities (Figs. 1, 6 and 7) [16,19], making it a typical type I FADS. However, kinetic parameters for its RFK and FMNAT activities expose some particularities (Tables 1 and 2). Thus, (i) the RFK activity is not inhibited by the RF substrate (as for *Ca*FADS) and takes place under oxidizing and reducing conditions—with the catalytic efficiency differring between both situations—(Fig. 3) and (ii) also unlike *Ca*FADS [22–24], but similarly to *Spn*FADS [16], its FMNAT activity requires reducing conditions (Fig. 4). Comparative studies of *Ca*FADS and *Spn*FADS envisaged that organisms can use different strategies at this enzyme level to keep flavin homeostasis; while *Ca*FADS carries out an inhibitory regulation of the RFK activity to control FAD production, the *Spn*FADS FMNAT activity is controled by the redox conditions of the environment [16,26]. Here, we further show that *Lm*FADS-1 modulates its RFK activity according to the oxidizing/reducing medium, while its FMNAT reaction depends on the availability of a reductant. Nevertheless, when evaluating what the reducing agent is needed for, we find differences. *Spn*FADS only binds flavinic substrates when they are reduced [16], while *Lm*FADS-1 binds them also under oxidizing conditions (Figs. 2 and 5, Table SP1). This suggests that the flavin binding site shape might differ between these two proteins. *Lm*FADS-1 would be able to accommodate both the oxidized (flat) and the reduced (bendable) isoalloxazine rings. On the contrary, in *Spn*FADS, only the reduced flavin ring appears to fit. Therefore, in *Lm*FADS-1, the flavin reduction would rather play a role in the correct organization of the catalytic transition state than in the initial substrate binding. In addition, free energy diagrams for ligands binding to the *Ca*FADS, *Spn*FADS, and *Lm*FADS-1 RFK modules highly differ (compare Fig. 5 with Fig. SP5 [26,27]). These diagrams suggest that substrates binding to *Lm*FADS-1 and *Spn*FADS take place through a random mechanism, while *Ca*FADS requires the RF and ATP concerted fit. In agreement, the 3D *Lm*FADS-1 model generated with *Spn*FADS leaves the adenine nucleotide binding site open and the PTAN motif ready to stabilize the ATP ligand, but the model generated with *Ca*FADS would show a conformation where the ATP binding site is closed (Fig. 6). This later conformation has been related to the substrate inhibition of the RFK activity in *Ca*FADS [27]. Since *Lm*FADS-1 does not show inhibition by substrate, we can assume that it will be structurally more similar to *Spn*FADS. Nevertheless, while formation of the ternary catalytic complex is the thermodynamically most favored process in *Spn*FADS—lowest positions in the energy diagram—other non-productive complexes, as FADS:FMN:ATP, are more stable for *Ca*FADS and *Lm*FADS-1. This envisages a higher degree of regulation by products in these two enzymes regarding *Spn*FADS. On the other hand, *Lm*FADS-2 has the typical structural

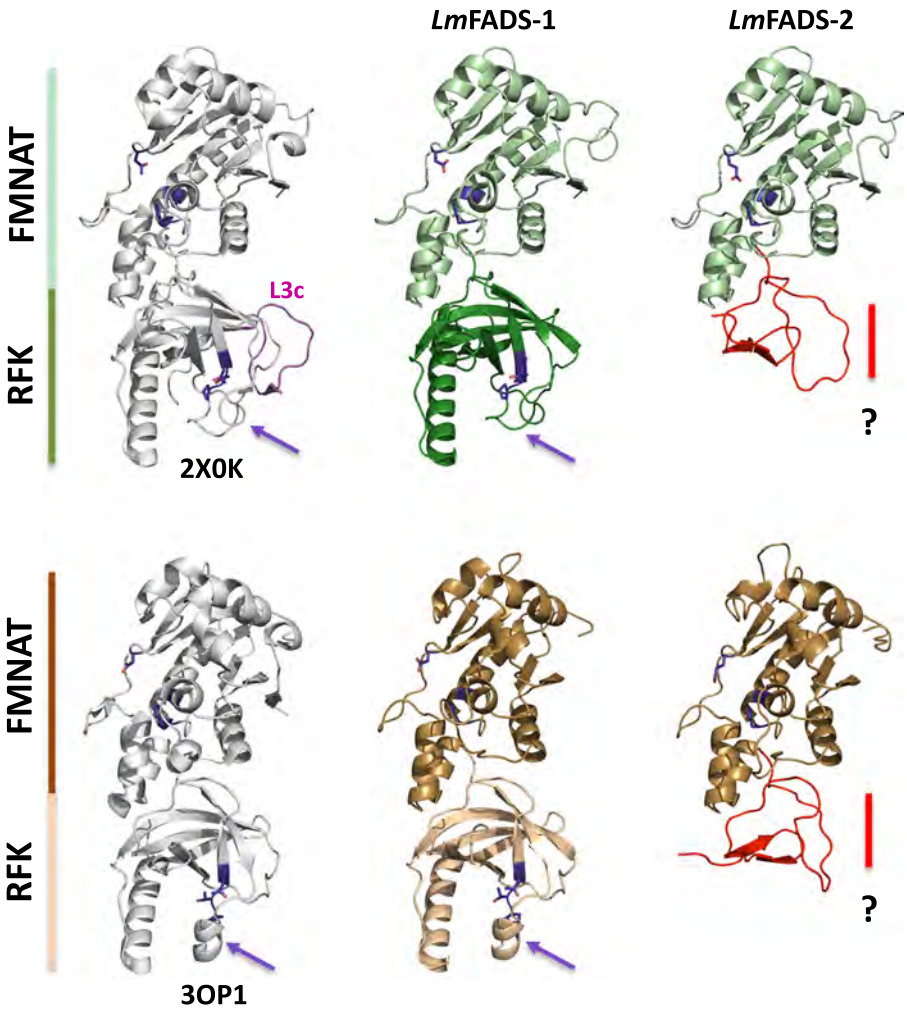

Fig. 6. Overall folding of *Lm*FADS-1 and *Lm*FADS-2 homology models. The figure shows cartoon models produced for each variant when using Modeller and either *Ca*FADS (models in greens) or *Spn*FADS (models in browns) templates. For each model, the FMNAT and RFK modules are highlighted by different color intensity. Structures for *Ca*FADS (pdb 2X0K, with the L3c extension in pink) and *Spn*FADS (pdb 3OP1) templates are shown in gray and compared to their corresponding models. Key active site residues at the FMNAT and RFK modules are highlighted in sticks and magenta colored. Main folding differences in secondary structure at the RFK module are pointed by an arrow. Models of *Lm*FADS-2 show in red the unstructured and structurally unpredictable C-terminal module.

elements related to the FMNAT activity at the N-terminal module but lacks those for the RFK activity at the C-terminal module for which a clear structural prediction is not possible (Fig. 6). CD results point to the same direction, with low contribution of β-sheet (Fig. 1). We identified the FMNAT activity for *Lm*FADS-2 and we can assert that its C-terminal module does not carry out the RFK activity. Consequently, its function, if any, remains unknown. Interestingly, *Lm*FADS-2 transforms FMN into FAD under both oxidizing and reducing environments (Fig. 4, Table 2), being the efficiency 2-fold higher under oxidizing conditions. In addition, qualitatively analysis by difference spectroscopy envisages *Lm*FADS-2 behaving differently from type I FADSs regarding binding of flavins (Fig. 2) [23,34].

*Lm*FADS-1 and *Lm*FADS-2 kinetic parameters considerably differ with the redox environment (Tables 1 and 2, Figs. 3 and 4). This resulted in FMN supply by *Lm*FADS-1 being highly dependent on both the concentration of substrates and the reducing environment. Thus, at low RF concentration, FMN production would be favored in an oxidizing environment, while at high RF concentrations, its transformation will be more efficient under reducing conditions (Fig. 3a). The theoretical models of *L. monocytogenes* FADSs produced, despite conservation in key catalytic residues, envisage a completely different surface electrostatic potential at the *Lm*FADS-1 and *Lm*FADS-2 FMNAT sites and, as a consequence, specific interplays with ligands (Fig. SP6A). It should be also noted that

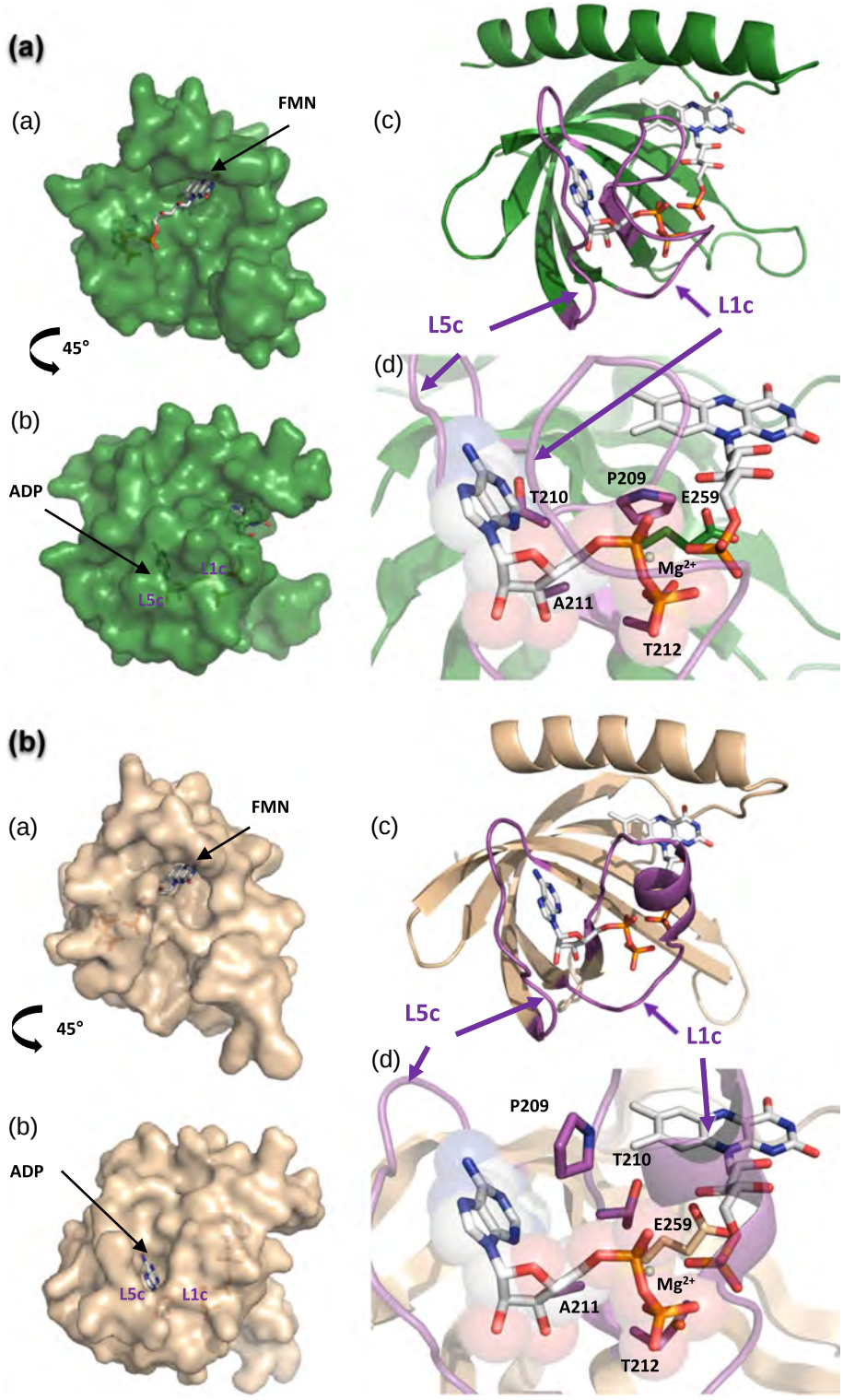

Fig. 7. 3D homology models of the RFK module of *Lm*FADS-1. Models based on the apo forms of (a) *Ca*FADS (green) and (b) *Spn*FADS (wheat). For each model, the different panels show (a) surface representation of the flavin binding site, (b) surface representation of the adenine nucleotide binding site, (c) loops L1c and L5c (in magenta) conforming the adenine nucleotide binding site, and (d) zoom into the putative conformation of the active site, showing in sticks the side-chains of the PTAN motif (magenta) interacting with ADP and Mg^{2+} and the catalytic base E259. The position of the ADP and FMN products (in white sticks) of the RFK activity and of the Mg^{2+} cation (small white sphere) has been modeled on the base of the *Ca*FADS-RFK:ADP:Mg^{2+}:FMN crystal structure (pdb 5A89).

*Lm*FADS-1 does not have inhibition by excess of RF. This, together with the fact that *L. monocytogenes* has two different enzymes for transforming FMN into FAD but *Lm*FADS-1 only operating under reducing conditions, suggests that both might have evolved to guarantee FMN and FAD supply under different energetic and redox environments. Considering that *L. monocytogenes* is a facultative anaerobic organism and an intracellular pathogen that populates different ecological niches, these two FMNAT modules might not be redundant to guarantee FAD supply under a broad range of conditions. This agrees with the presence of conserved homologs providing adaptative beneficts to bacteria [35], and particularly with specie-specific traits and FMN/FAD requirements under the different lifestyles that *L. monocytogenes* populates from saprophytism to virulence. We should also add that these bacteria contain a single FMN riboswitch, Rli96, with the downstream gene encoding a RF key transporter for their growth [11,36]. Thus, the FMN homeostasis reached by *Lm*FADS-1 and *Lm*FADS-2 migth play also a role in the control of RF import under diverse bacterial growth conditions.

Type I and type II FADSs are common to all known *Listeria* species (Fig. SP7–SP8). Type I *Listeria* FADSs are relatively conserved (Fig. SP7), whereas type II proteins have lower sequence identity at the FMNAT region and the homology of the C-terminal region is reduced to just a few motives (Fig. SP8). Our analysis fails to reveal a reliable structural/functional model for the *Lm*FADS-2 C-terminal. In addition, although most bacteria are able to synthesize RF, there exist some species that (i) uptake external RF using specialized flavin transport systems or (ii) conserve both RF biosynthesis and uptake functions [37]. *Listeria* and different *Lactobacillus* species and strains belong to the auxotrophic group [38,39]. Interestingly, type II FADSs, rare among bacterial species, are found in *Listeria* and other Firmicutes phyla, such as *Lactobacillus* (Fig. SP9) or *Bacillus cereus* [15]. Thus, although RF supply pathways have been extensively investigated, some steps remain unknown and in many cases pathways are specific of specie, being therefore the metabolism of flavins highly adaptative to fulfill each species needs [37]. *L. monocytogenes* strains classify in at least four evolutionary lineages, with genetic and phenotypic characteristics, found in different but overlaping ecological niches and serotypes, and differently associated with their ability to be transmitted through foods and to cause human disease [8]. Nonetheless, *Lm*FADS-1 and *Lm*FADS-2 sequences are highly conserved within the more than 100 *L. monocytogenes* strains so far identified (Table SP2) [8], with divergences only found in a few strains and affecting to a small number of residues (Tables SP3 and SP4) predicted at the protein surface and far from active sites (Fig. SP6B).

In conclusion, although diversifying selection in FADS enzymes does not appear key in *L. monocytogenes* lineages evolution, the presence of type I and type II FADSs is not redundant in *Listeria* species. In these organisms, the combined action of these two FADSs is envisaged to ensure flavins supply under different environmental conditions. Furthermore, the data here presented confirm that FADSs in bacteria seem to be diverse in catalytic requirements, facts that appear strongly dependent on species-specific physiological traits.

Materials and Methods

Biological material

The *L. monocytogenes* HCC23 (NC_011660.1) LMHCC_RS06360, and LMHCC_RS09565 genes [40], respectively, codifying for *Lm*FADS-1 (WP_012581380.1) and *Lm*FADS-2 (WP_012581760.1), were retrieved from GenScript services and cloned into the pHAT2 plasmid, incorporating a His_6-Tag sequence at the N-terminal. Competent *E. coli* BL21 (DE3) Star cells were transformed with pHAT2-*Lm*FADS-1 or pHAT2-*Lm*FADS-2 expression plasmid and inoculated into precultured of 20–40–20 growth medium (20 g/l glycerol, 40 g/l yeast extract, 20 g/l tryptone) which contained 100 ml of buffer (70 g/l KH_2PO_4, 70 g/l Na_2PO_4, and 50 g/l NaCl) and 50 μg/ml ampicillin as selection antibiotic. Cells were incubated at 30 °C up to the early stationary phase (OD_{600} 5–6), and then chilled, and decanted overnight at 4 °C. The pellet was inoculated into 1.5 l of High Density Medium at a starting OD_{600} of 0.8 to 1 (Table SP5) [41]. Cultures were grown in 2-l fermentor (Bioflo3000 New Brunswick) at 30 °C with dissolved oxygen concentration above 80% of air saturation until reaching the OD_{600} of 20. Temperature was then rapidly lowered to 14 °C before protein expression induced through addition of 1 mM IPTG. The culture was further incubated overnight (15 to 18 h) at the same temperature. Cells were harvested by centrifugation and stored at −20 °C. In order to purifiy the overexpressed proteins, cells were resuspended and sonicated in the lysis buffer previously described [19] containing 0.5 mM DTT. The supernatant was then fractionated with 20% ammonium sulfate. The pellet was discarded and the supernatant loaded onto a Phenyl-Sepharose high-performance column equilibrated with Tris/HCl 50 mM (pH 8.0) and 20% ammonium sulphate. The column was washed until elution of the flavin, and then a lineal 20%–0% ammonium sulfate gradient was applied. The fractions containing the protein were pooled and half-diluted in 20 mM Pipes (pH 7.0) at 4 °C. The protein was then loaded onto a Ni^{2+}-IMAC column (HiTRAP™ Chelating HP 5 ml, GE Healthcare)

equilibrated with 20 mM Pipes (pH 7.0) and eluted through a 0- to 300-mM imidazole gradient. Fractions containing *Lm*FADS-1 or *Lm*FADS-2 were pooled and dialyzed in 20 mM Pipes and 1 mM DTT (pH 7.0), with 50 mM and 20 mM imidazole, respectively, and stored at 4 °C.

Size distribution analysis

A Superdex 200 10/300 (GE Healthcare) gel filtration chromatography column, previously equilibrated with 20 mM Pipes (pH 7.0) and calibrated with the Gel Filtration Calibration Kit LMW (GE Healthcare), was used to separate the different species by their size as previously described [23,32,34]. Chromatograms were fit to a set of Gaussian functions (Origin7.0, OriginLab) to determine the number of components, their percentages and their estimated masses [32,34].

Spectral analysis

Molar extinction coefficients for *Lm*FADS-1 and *Lm*FADS-2 ($\varepsilon_{279\ nm}$) were determined in 20 mM Pipes (pH 7.0) with 50 mM and 20 mM imidazole, respectively ([49]). CD spectra were recorded in a Chirascan spectropolarimeter (Applied Photophysics Ltd.) at 25 °C. Far-UV spectra were registered in 0.1-cm path length cuvettes with samples containing ~5 μM protein in 5 mM Pipes (pH 7.0). Near-UV spectra were measured in 0.4-cm path length cuvettes with samples containing ~20 μM protein in 20 mM Pipes (pH 7.0). UV–Vis difference spectra were registered in 20 mM Pipes and 0.8 mM $MgCl_2$ (pH 7.0) in the presence of saturating substrate concentrations, as previously described [20,24].

Qualitative detection of *Lm*FADS-1 and *Lm*FADS-2 activities

RFK, FMNAT, and FADpp activities were qualitatively assayed by separation of flavins from reaction mixtures using TLC. Reaction mixtures containing 50 μM RF, FMN or FAD, and 0.2 mM ATP or PPi, in 20 mM Pipes, 0.8 or 10 mM $MgCl_2$, were incubated with ~200 nM FADS for 15, 30, or 120 min at 37 °C. Reactions were stopped by heating the mixtures at 100 °C for 5 min and applied to 20 × 20-cm Silica Gel SIL-G-25 plates, with a thickness of 0.25 mm [19]. Flavin spots were examined determining their fluorescence under UV light. When required sodium dithionite was used as flavin reducing agent.

Steady-state kinetics parameters for the RFK and FMNAT activities

The RFK and FMNAT activities were quantitatively determined at 25 °C through high-performance liquid chromatography, as previously described [17,24]. The RFK activity was determined by quantifying the RF transformed when mixing 25–40 nM protein with reaction mixtures containing 0.2–50 μM RF, 10–450 μM ATP in 20 mM Pipes, and 0.8 mM $MgCl_2$ (pH 7.0). The FMNAT activity was similarly measured, but in this case, the FAD produced from FMN was determined. The reaction mixtures contained 0.2–160 μM FMN, 10–500 μM ATP in 20 mM Pipes, and 0.8 mM $MgCl_2$. Reactions started by adding 70–160 nM protein. Activities were measured in a final volume of 500 μl. All reaction mixtures were incubated 1 min at 25 °C after adding the enzyme, and the reaction was stopped by heating at 100 °C for 5 min. All experiments were carried out both in the absence and presence of sodium dithionite (24 mM). When sodium dithionite was present, it was added to the reaction mixture after it was bubbled with and oxygen-free gas for 20 min and equilibrated at the working temperature. The sodium dithionite concentration was ment (i) to obtain data comparable to those reported for FADSs from a different *L. monocytogenes* strain [11] and (ii) to ensure fast removal of the oxygen contained in the protein solution without the need of bubbling (to avoid its deterioration). Kinetic data obtained when varying the concentration of one of the substrates while keeping constant and saturating the other one were fitted to the Michaelis–Menten equation.

High-sensitivity ITC

To determine the interaction of *Lm*FADS-1 with its ligands, ITC measurements were performed using an AutoITC 200 calorimeter (MicroCal-Malvern) thermostated at 15 °C, following procedures previously reported [24,26,27]. Typically, 300 μM nucleotide or 150–200 μM flavin solutions were used to titrate ~25 μM *Lm*FADS-1 solutions. When appropriate, ternary titrations were performed by adding flavin solutions to a mixture of the protein preincubated with 400 μM ADP. The ligands and *Lm*FADS-1 were dissolved in 20 mM Pipes (pH 7.0) and 7 mM imidazole, with 0 or 0.8 $MgCl_2$, and degassed prior to titration. Up to 19 injections of 2 μl of the titrating ligand were added to the sample cell. The association constant (K_a), the enthalpy change (ΔH), and the stoichiometry (N) were estimated through non-linear regression of the experimental data using a model for one binding site implemented in Origin 7.0 (OriginLab). The dissociation constant (K_d), the free energy change (ΔG), and the entropy change (ΔS) were obtained from basic thermodynamic relations. Cooperative binding phenomena between adenine and flavin nucleotides were determined using ITC as previously described [26,27]. In brief, to determine the cooperativity coefficients (α) describing the interactions between the ANP and the FLV ligands, a set of six additional experiments was carried out. Mixtures containing *Lm*FADS-1 at six different FLV

concentrations were titrated with ANP ligands. These experiments allowed the determination of the apparent association constants for the adenine nucleotide ligand, $K_a^{app,\ ANP}$, at each particular concentration of the FLV ligand mixed with the protein in the calorimetric cell. The data were fit to the equation describing the dependency of $K_a^{app,\ ANP}$ as a function of the FLV concentration and α (cooperativity constant for the heterotropic interaction between ANP and FLV) $K_a^{app,ANP} = K_a^{ANP} \frac{1 + \alpha\, K_a^{FLV}\,[FLV]}{1 + K_a^{FLV}\,[FLV]}$; where K_a^{ANP} is the association constant for ANP, K_a^{FLV} is the association constant for FLV, and [FLV] is the concentration of flavin in the calorimetric cell. All titrations were performed in triplicate. The errors considered in the measured parameters (±15% in K_d and K_a values, ± 0.3 kcal mol^{-1} in ΔG, ΔH and $-T\Delta S$ and ±20% in α) were assumed to be larger than the standard deviation between replicates and the numerical error after fitting analysis.

Sequence alignment and structural modeling

FADS type II sequences in 19 *Listeria* species and *Lm*FADS-1 and *Lm*FADS-2 sequences of 118 complete assembly genomes of *L. monocytogenes* serotypes were retrieved from NCBI Microbial Reference Sequence Database (https://www.ncbi.nlm.nih.gov/genome/microbes/) and NCBI RefSeq Data Bank (https://www.ncbi.nlm.nih.gov/assembly), respectively, using PSI-BLAST [42]. Multiple sequence alignments were done with Clustal Omega (https://www.ebi.ac.uk/Tools/msa/clustalo/). Secondary structure predictions were made with PSIPRED [43] and sequence logo representations were created with WebLogo_3 tool (http://weblogo.berkeley.edu/logo.cgi). 3D structural modeling of *Lm*FADS-1 and *Lm*FADS-2 was driven with HHPred (https://toolkit.tuebingen.mpg.de/) and Modeller [44,45] using the apo x-ray structures of *Ca*FADS (PDB ID: 2X0K) [22] and *Spn*FADS (PDB ID: 3OP1) as templates. Structures and models were inspected, analyzed and plotted with PyMol 1.4.1 (Schrodinger LLC). Prediction of disordered residues (IDRs) was done with PONDR VSL2b [46,47], and Molecular Recognition Feature (MoRF) prediction was done with MoRFpred tool http://biomine.cs.vcu.edu/servers/MoRFpred/ [48].

Acknowledgments

This work has been supported by the Spanish Ministry of Economy, Industry and Competitiveness (MINECO) (BIO2016-75183-P AEI/FEDER, UE, to M.M.) and the Government of Aragón-FEDER (E35_17R to M.M.). We thank Dr. A. Velázquez-Campoy for help in analysis and discussion regarding the ITC data.

Author Contributions: M.M., conceptualization, funding acquisition, supervision, writting, review and editing. M.S., investigation, methodology, formal analysis, original draft. S.A., investigation. J.B., investigation. I.Y., investigation, formal analysis, methodology, writing.

Author Disclosure Statement: No competing financial interests exist.

Appendix A. Supplementary data

Supplementary data to this article can be found online at https://doi.org/10.1016/j.jmb.2019.05.029.

Received 19 February 2019;
Received in revised form 20 May 2019;
Available online 25 May 2019

Keywords:
FMN and FAD biosynthesis;
riboflavin kinase;
FMN:ATP adenylyltransferase;
FAD synthase;
Listeria monocytogenes

Abbreviations used:
FADS, FAD synthase; FMN, flavin mononucleotide; FAD, flavin adenine dinucleotide; *Ca*FADS, FADS from *Corynebacterium ammoniagenes*; *Spn*FADS, FADS from *Streptococcus pneumoniae*; RFK, ATP:riboflavin kinase; FMNAT, ATP:FMN adenylyltransferase; *Lm*FADS-1, type I FAD synthase from *Listeria monocytogenes* HCC23; *Lm*FADS-2, type II FAD synthase from *Listeria monocytogenes* HCC23.

References

[1] B. Swaminathan, P. Gerner-Smidt, The epidemiology of human listeriosis, Microbes Infect. 9 (2007) 1236–1243.
[2] K. Dhama, K. Karthik, R. Tiwari, M.Z. Shabbir, S. Barbuddhe, S. V. Malik, et al., Listeriosis in animals, its public health significance (food-borne zoonosis) and advances in diagnosis and control: a comprehensive review, Vet Q. 35 (2015) 211–235.
[3] S. Lomonaco, D. Nucera, V. Filipello, The evolution and epidemiology of *Listeria monocytogenes* in Europe and the United States, Infect. Genet. Evol. 35 (2015) 172–183.
[4] B. Smith, M. Kemp, S. Ethelberg, P. Schiellerup, B.G. Bruun, P. Gerner-Smidt, et al., *Listeria monocytogenes*: maternal-foetal infections in Denmark 1994–2005, Scand. J. Infect. Dis. 41 (2009) 21–25.
[5] R. Wadhwa Desai, M.A. Smith, Pregnancy-related listeriosis, Birth Defects Res. 109 (2017) 324–335.
[6] J.A. Vázquez-Boland, M. Kuhn, P. Berche, T. Chakraborty, G. Domínguez-Bernal, W. Goebel, et al., Listeria pathogenesis and molecular virulence determinants, Clin. Microbiol. Rev. 14 (2001) 584–640.

[7] J.R. Donaldson, B. Nanduri, J.R. Pittman, S. Givaruangsawat, S.C. Burgess, M.L. Lawrence, Proteomic expression profiles of virulent and avirulent strains of *Listeria monocytogenes* isolated from macrophages, J. Proteome 74 (2011) 1906–1917.
[8] R.H. Orsi, H.C. den Bakker, M. Wiedmann, *Listeria monocytogenes* lineages: genomics, evolution, ecology, and phenotypic characteristics, Int J Med Microbiol. 301 (2011) 79–96.
[9] A.C. Camargo, J.J. Woodward, L.A. Nero, The continuous challenge of characterizing the foodborne pathogen *Listeria monocytogenes*, Foodborne Pathog. Dis. 13 (2016) 405–416.
[10] M.A. Mraheil, A. Billion, W. Mohamed, K. Mukherjee, C. Kuenne, J. Pischimarov, et al., The intracellular sRNA transcriptome of *Listeria monocytogenes* during growth in macrophages, Nucleic Acids Res. 39 (2011) 4235–4248.
[11] A. Matern, D. Pedrolli, S. Großhennig, J. Johansson, M. Mack, Uptake and metabolism of antibiotics roseoflavin and 8-demethyl-8-aminoriboflavin in riboflavin-auxotrophic *Listeria monocytogenes*, J. Bacteriol. 198 (2016) 3233–3243.
[12] H.J. Welshimer, Vitamin requirements of *Listeria monocytogenes*, J. Bacteriol. 85 (1963) 1156–1159.
[13] A. Gutiérrez-Preciado, A.G. Torres, E. Merino, H.R. Bonomi, F.A. Goldbaum, V.A. García-Angulo, Extensive identification of bacterial riboflavin transporters and their distribution across bacterial species, PLoS One 10 (2015), e0126124.
[14] A.G. Vitreschak, D.A. Rodionov, A.A. Mironov, M.S. Gelfand, Regulation of riboflavin biosynthesis and transport genes in bacteria by transcriptional and translational attenuation, Nucleic Acids Res. 30 (2002) 3141–3151.
[15] I. Yruela, S. Arilla-Luna, M. Medina, B. Contreras-Moreira, Evolutionary divergence of chloroplasts FAD synthetase proteins, BMC Evol. Biol. 10 (2010) 311.
[16] M. Sebastián, E. Lira-Navarrete, A. Serrano, C. Marcuello, A. Velázquez-Campoy, A. Lostao, et al., The FAD synthetase from the human pathogen *Streptococcus pneumoniae*: a bifunctional enzyme exhibiting activity-dependent redox requirements, Sci. Rep. 7 (2017) 7609.
[17] A. Serrano, S. Frago, A. Velázquez-Campoy, M. Medina, Role of key residues at the flavin mononucleotide (FMN): adenylyltransferase catalytic site of the bifunctional riboflavin kinase/flavin adenine dinucleotide (FAD) Synthetase from *Corynebacterium ammoniagenes*, Int. J. Mol. Sci. 13 (2012) 14492–14517.
[18] I. Efimov, V. Kuusk, X. Zhang, W.S. McIntire, Proposed steady-state kinetic mechanism for *Corynebacterium ammoniagenes* FAD synthetase produced by *Escherichia coli*, Biochemistry. 37 (1998) 9716–9723.
[19] S. Frago, M. Martínez-Júlvez, A. Serrano, M. Medina, Structural analysis of FAD synthetase from *Corynebacterium ammoniagenes*, BMC Microbiol. 8 (2008) 160.
[20] S. Frago, A. Velázquez-Campoy, M. Medina, The puzzle of ligand binding to *Corynebacterium ammoniagenes* FAD synthetase, J. Biol. Chem. 284 (2009) 6610–6619.
[21] B. Herguedas, I. Lans, M. Sebastián, J.A. Hermoso, M. Martínez-Júlvez, M. Medina, Structural insights into the synthesis of FMN in prokaryotic organisms, Acta Crystallogr D Biol Crystallogr. 71 (2015) 2526–2542.
[22] B. Herguedas, M. Martinez-Julvez, S. Frago, M. Medina, J.A. Hermoso, Oligomeric state in the crystal structure of modular FAD synthetase provides insights into its sequential catalysis in prokaryotes, J. Mol. Biol. 400 (2010) 218–230.
[23] A. Serrano, M. Sebastian, S. Arilla-Luna, S. Baquedano, M.C. Pallares, A. Lostao, et al., Quaternary organization in a bifunctional prokaryotic FAD synthetase: involvement of an arginine at its adenylyltransferase module on the riboflavin kinase activity, Biochim. Biophys. Acta 1854 (2015) 897–906.
[24] A. Serrano, S. Frago, B. Herguedas, M. Martinez-Julvez, A. Velazquez-Campoy, M. Medina, Key residues at the riboflavin kinase catalytic site of the bifunctional riboflavin kinase/FMN adenylyltransferase from *Corynebacterium ammoniagenes*, Cell Biochem. Biophys. 65 (2013) 57–68.
[25] A. Serrano, P. Ferreira, M. Martínez-Júlvez, M. Medina, The prokaryotic FAD synthetase family: a potential drug target, Curr. Pharm. Des. 19 (2013) 2637–2648.
[26] M. Sebastián, A. Serrano, A. Velázquez-Campoy, M. Medina, Kinetics and thermodynamics of the protein-ligand interactions in the riboflavin kinase activity of the FAD synthetase from *Corynebacterium ammoniagenes*, Sci. Rep. 7 (2017) 7281.
[27] M. Sebastián, A. Velázquez-Campoy, M. Medina, The RFK catalytic cycle of the pathogen *Streptococcus pneumoniae* shows species-specific features in prokaryotic FMN synthesis, J Enzyme Inhib Med Chem. 33 (2018) 842–849.
[28] S. Grill, S. Busenbender, M. Pfeiffer, U. Kohler, M. Mack, The bifunctional flavokinase/flavin adenine dinucleotide synthetase from *Streptomyces davawensis* produces inactive flavin cofactors and is not involved in resistance to the antibiotic roseoflavin, J. Bacteriol. 190 (2008) 1546–1553.
[29] E.B. Kearney, J. Goldenberg, J. Lipsick, M. Perl, Flavokinase and FAD synthetase from *Bacillus subtilis* specific for reduced flavins, J. Biol. Chem. 254 (1979) 9551–9557.
[30] M. Barile, T.A. Giancaspero, P. Leone, M. Galluccio, C. Indiveri, Riboflavin transport and metabolism in humans, J. Inherit. Metab. Dis. 39 (2016) 545–557.
[31] N. Leulliot, K. Blondeau, J. Keller, N. Ulryck, S. Quevillon-Cheruel, H. van Tilbeurgh, Crystal structure of yeast FAD synthetase (Fad1) in complex with FAD, J. Mol. Biol. 398 (2010) 641–646.
[32] C. Marcuello, S. Arilla-Luna, M. Medina, A. Lostao, Detection of a quaternary organization into dimer of trimers of *Corynebacterium ammoniagenes* FAD synthetase at the single-molecule level and at the in cell level, Biochim. Biophys. Acta 1834 (2013) 665–676.
[33] I. Yruela, B. Contreras-Moreira, C. Magalhães, N.S. Osório, J. Gonzalo-Asensio, *Mycobacterium tuberculosis* complex exhibits lineage-specific variations affecting protein ductility and epitope recognition, Genome Biol Evol. 8 (2016) 3751–3764.
[34] A. Serrano, M. Sebastián, S. Arilla-Luna, S. Baquedano, B. Herguedas, A. Velázquez-Campoy, et al., The trimer interface in the quaternary structure of the bifunctional prokaryotic FAD synthetase from *Corynebacterium ammoniagenes*, Sci. Rep. 7 (2017) 404.
[35] M. Mærk, J. Johansen, H. Ertesvåg, F. Drabløs, S. Valla, Safety in numbers: multiple occurrences of highly similar homologs among *Azotobacter vinelandii* carbohydrate metabolism proteins probably confer adaptive benefits, BMC Genomics 15 (2014) 192.
[36] M. Mansjo, J. Johansson, The riboflavin analog roseoflavin targets an FMN-riboswitch and blocks *Listeria monocytogenes* growth, but also stimulates virulence gene-expression and infection, RNA Biol. 8 (2011) 674–680.
[37] V.A. García-Angulo, Overlapping riboflavin supply pathways in bacteria, Crit. Rev. Microbiol. 43 (2017) 196–209.
[38] H. Marquis, H.G. Bouwer, D.J. Hinrichs, D.A. Portnoy, Intracytoplasmic growth and virulence of *Listeria*

monocytogenes auxotrophic mutants, Infect. Immun. 61 (1993) 3756–3760.
[39] K. Thakur, S.K. Tomar, B. Brahma, S. De, Screening of riboflavin-producing lactobacilli by a polymerase-chain-reaction-based approach and microbiological assay, J. Agric. Food Chem. 64 (2016) 1950–1956.
[40] C.L. Steele, J.R. Donaldson, D. Paul, M.M. Banes, T. Arick, S.M. Bridges, et al., Genome sequence of lineage III *Listeria monocytogenes* strain HCC23, J. Bacteriol. 193 (2011) 3679–3680.
[41] E. Frachon, V. Bondet, H. Munier-Lehmann, J. Bellalou, Multiple microfermentor battery: a versatile tool for use with automated parallel cultures of microorganisms producing recombinant proteins and for optimization of cultivation protocols, Appl. Environ. Microbiol. 72 (2006) 5225–5231.
[42] S.F. Altschul, T.L. Madden, A.A. Schäffer, J. Zhang, Z. Zhang, W. Miller, et al., Gapped BLAST and PSI-BLAST: a new generation of protein database search programs, Nucleic Acids Res. 25 (1997) 3389–3402.
[43] D.T. Jones, Protein secondary structure prediction based on position-specific scoring matrices, J. Mol. Biol. 292 (1999) 195–202.
[44] R. Sánchez, A. Sali, Evaluation of comparative protein structure modeling by MODELLER-3, Proteins. 1 (1997) 50–58 Suppl.
[45] L. Zimmermann, A. Stephens, S.Z. Nam, D. Rau, J. Kübler, M. Lozajic, et al., A completely reimplemented MPI bioinformatics toolkit with a new HHpred server at its Core, J. Mol. Biol. 430 (2018) 2237–2243.
[46] Z.L. Peng, L. Kurgan, Comprehensive comparative assessment of in-silico predictors of disordered regions, Curr. Protein Pept. Sci. 13 (2012) 6–18.
[47] K. Peng, P. Radivojac, S. Vucetic, A.K. Dunker, Z. Obradovic, Length-dependent prediction of protein intrinsic disorder, BMC Bioinformatics. 7 (2006) 208.
[48] F.M. Disfani, W.L. Hsu, M.J. Mizianty, C.J. Oldfield, B. Xue, A.K. Dunker, et al., MoRFpred, a computational tool for sequence-based prediction and characterization of short disorder-to-order transitioning binding regions in proteins, Bioinformatics. 28 (2012) i75–i83.
[49] P. Macheroux, UV-visible spectroscopy as a tool to study flavoproteins, Methods Mol Biol. 131 (1999) 1–7.